2023

Streaming and zeta potentials of basalt as a function of pressure, temperature, salinity, and pH

Mirhasan Hosseini
Edith Cowan University

Faisal Ur Rahman Awan
Edith Cowan University

Nilesh Kumar Jha
Edith Cowan University

Alireza Keshavarz
Edith Cowan University

Stefan Iglauer
Edith Cowan University

10.1016/j.fuel.2023.128996
Hosseini, M., Awan, F. U. R., Jha, N. K., Keshavarz, A., & Iglauer, S. (2023). Streaming and zeta potentials of basalt as a function of pressure, temperature, salinity, and pH. *Fuel*, *351*, article 128996. https://doi.org/10.1016/j.fuel.2023.128996

Fuel 351 (2023) 128996

Contents lists available at ScienceDirect

Fuel

journal homepage: www.elsevier.com/locate/fuel

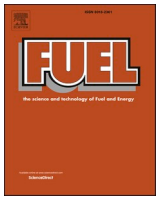

Full Length Article

Streaming and zeta potentials of basalt as a function of pressure, temperature, salinity, and pH

Mirhasan Hosseini *, Faisal Ur Rahman Awan, Nilesh Kumar Jha, Alireza Keshavarz, Stefan Iglauer

Petroleum Engineering Discipline, School of Engineering, Edith Cowan University, 270 Joondalup Dr, Joondalup, 6027, WA, Australia

ARTICLE INFO

Keywords:
Zeta potential
Streaming potential
Basalt
Dead brine
Live brine
High pressure

ABSTRACT

The electric surface charge of basalt in contact with filing fluids (e.g. water and CO_2) has broad range of applications in varied fields such as gas geological storage sites, geothermal systems, and hydrocarbon reservoirs. The surface charge at the interface between a solid surface (e.g. rock) and liquid (e.g. aqueous solution) can be quantified by the zeta potential, thus zeta potential measurement is a useful technique for interpreting wetting characteristics of rock-fluid systems. However, there is no data for zeta potentials of basaltic rocks in presence of aqueous solutions or how zeta potentials may be affected by pressure, temperature, salinity, or pH. Thus, streaming potential measurements were performed to determine the zeta potential of basaltic rocks in the presence of aqueous NaCl solution at pore pressures (1.72 MPa to 6.9 MPa), temperatures (298 K and 323 K), brine salinities (1 wt% NaCl to 3.5 wt% NaCl), and pH values (4 to 10). Also, the effects of mineralogy and CO_2-presence (dead and live brines) on the zeta potential were evaluated. The results showed that the zeta potential remained constant versus pressure, while it increased (became less negative) with increasing temperature and salinity, and decreased (became more negative) with increasing pH. This study provides key fundamental data and thus improves fundamental understanding of basalt-water-CO_2 interactions, thereby aiding in the improvement of various industrial applications, including gas geo-storage schemes and geothermal energy production.

1. Introduction

Basalt is the most common igneous rock in Earth's crust; it constitutes 67% of the ocean floor (with 2–4 km thick layers), and covers 10% of the continents' surfaces [1–4]. Such basaltic formations may form groundwater aquifers, geothermal reservoirs or hydrocarbon reservoirs [5–10]. However, while fluid flow through sedimentary rocks (e.g. carbonates or sandstones) has been widely investigated (e.g. [11–14]), fluid flow through basaltic rocks is only poorly understood [15]. One key property related to such fluid flow is the streaming potential C (which is created when an electrolyte (here brine) flows through a stationary porous medium (here basalt) [16,17]). C has a broad spectrum of important applications, including in enhanced hydrocarbon recovery, geothermal engineering, volcanology, drinking water production, hydraulic fracturing, CO_2 geo-sequestration (CGS) and H_2 geo-storage (e.g. [18–23]). C is related to the zeta potential (ζ) of the basalt, which is one of the main wettability-determinants and thus directly influences fluid flow through the basalt (e.g. [24–26]).

The ζ of sedimentary rocks has been widely investigated in the literature for various purposes. Regarding the influence of high salinity brines on ζ, Singh et al. (2022) [27], Collini et al. (2020) [18], Cherubini et al. (2018) [28], and Al Mahrouqi et al. (2017) [33] investigated carbonates, while Walker & Glover (2018) [29], Alarouj et al. (2021) [30], and Nasralla & Nasr-El-Din (2014) [31] examined sandstone. The effect of elevated temperature on ζ for carbonates was studied by Al Mahrouqi et al. (2016) [32], Al Mahrouqi et al. (2017) [33], and Rodríguez & Araujo (2006) [34], while Vinogradov & Jackson (2015) [35] investigated this effect for sandstone. In terms of conducting ζ measurements under multi-phase flow conditions, Revil & Cerepi (2004) [36] conducted tests on carbonates, while Sprunt et al. (1994) [17] studied carbonates and sandstone. Additionally, Alroudhan et al. (2016) [37] investigated the impact of brine composition on ζ for carbonates, and Thanh & Sprik (2016) [38] examined this effect for sandstone. The effect of brine pH on ζ for carbonates was examined by Vdović & Bišćan

* Corresponding author.
E-mail addresses: m.hosseini@ecu.edu.au, mirhasan.hosseini@gmail.com (M. Hosseini).

https://doi.org/10.1016/j.fuel.2023.128996
Received 2 April 2023; Received in revised form 29 May 2023; Accepted 11 June 2023
Available online 17 June 2023

(1998) [39], Vdović (2001) [40], Mahani et al. (2017) [22], and Chen et al. (2014) [41]. In the case of sandstone, Vinogradov & Jackson (2015) [35], Alarouj et al. (2021) [30], and Hidayat et al. (2022) [19] investigated this effect.

However, ζ of volcanic rocks received only little attention. For example, Jouniaux et al. (2000) [42] measured the zeta potential of 11 andesitic volcanic samples with different permeabilities and concluded that the increase in permeability of basalt results in an increase in C. They attributed this variation to the reduction of rock's effective conductivity with permeability (note: C has inverse relation with the effective conductivity (e.g. [43]), see section 2.3). In another study, Hase et al. (2003) [44] derived the zeta potential of various rocks from Aso volcano and found that basalt samples with low SiO_2 content and high isoelectric points (note: isoelectric point is the pH value where ζ equals zero [45]) showed positive zeta potentials (ζ ranged from −20 to + 20 mV). Moreover, Aizawa et al. (2008) [46] derived the zeta potential of 73 volcanic samples and found 9 samples with positive zeta potential, 11 samples with small values<10 mV, and the remaining samples with negative zeta potentials. There are also a few studies reporting ζ of the minerals which are commonly found in basaltic rocks, including augite [47], olivine [48], labradorite [49], albite [50], and microcline [51]. Under typical experimental conditions, most of these minerals have been found to exhibit negative zeta potentials.

Various thermophysical parameters, including pressure, temperature, brine salinity and composition (note that formation water always contains dissolved salts which can reach maximum saturation [52–56]), and brine pH can vary significantly in the underground [57,58], and this may significantly affect C and ζ [17,36,59,60]. However, the effects of these parameters on ζ of basaltic rock remains unknown.

In this study, we therefore examine the influence of pressure, temperature, pH value and brine salinity on ζ of a New Zealand basaltic rock sample. This also includes the effect of CO_2 (an acidic gas) added on ζ; this study will thus aid various important applications, including gas geo-storage (CO_2 and H_2) and geothermal projects.

2. Experimental methodology

2.1. Materials

A New Zealand basaltic core plug (petrophysical and mineralogical properties are listed in Table 1) was retrieved from Auckland Volcanic Field (AVF, depth = 74 m, age = 68.3 ka), New Zealand [61]. The sample contained labradorite ($(Na,Ca)_{1\text{-}2}Si_{3\text{-}2}O_8$), augite ($Ca(Fe,Mg)Si_2O_6$), olivine ($(Mg,Fe)_2SiO_4$), and nepheline ($(Na,K)AlSiO_4$) as main mineral components [61] (compare Table 1). Furthermore, aqueous NaCl solutions ("dead brines") were prepared by dissolving NaCl salt (purity ≥ 99 mol% from Scharlab) in deionized (DI) water (electrical conductivity of 0.02 $mS.cm^{-1}$ from David Gray). Small amounts of NaOH (purity ≥ 99 mol% from Scharlab) and (aqueous) HCl (concentration of 10^{-3} mol/L and purity ≥ 99 mol% from Scharlab) were added for adjusting pH values (measured via a FiveGo pH meter, Mettler Toledo, accuracy of 0.01 pH units). Live brine was also prepared by dissolving CO_2 (purity > 99.9 mol% from BOC) in the dead brine at HPHT conditions, see below. The compositions of the produced brines (after core flooding, see also below) were analyzed via inductively coupled plasma (ICP) tests using a HORIBA Jobin Yvon® ULTIMA 2C instrument.

Table 1
Petrophysical and mineralogical properties of the basalt sample used in this study.

Property	Result	Unit
Mineralogy[1]	Labradorite (42), Augite (37.5), Olivine (11.9), Nepheline (8.6)	wt %
Core plug dimensions	Length = 5.2, Diameter = 3.8	cm
Porosity[2]	10 ± 1.0	%
Brine permeability[3]	4.6 ± 0.3	mD
Formation factor (F)[4]	61 ± 2	–

[1] Measured via X-ray diffraction (XRD, Bruker-AXS D8 instrument) analysis [54].
[2] Measured via UltraPoroPerm-910 from Core Laboratories.
[3] Measured in core-flood apparatus (shown in Fig. 1). Permeability was measured at 10 MPa overburden pressure, and the error was obtained based on three different flow rates used at the same overburden pressure.
[4] $F = \sigma_w/\sigma_{rw}$ is used when surface electrical conductivity is negligible for salinities > 0.1 M (as assumed here, see section 2.3)[62].

2.2. Experimental procedure

The streaming potential experiments were conducted using an HPHT core flooding system, Fig. 1. The core sample was cleaned with toluene and methanol to remove any impurities that could interfere with the flow or alter the surface properties. The core holder with the sample inside and associated electrodes on two sides was placed inside an oven with controlled temperature (accuracy of ± 1 °C). The core holder is made of polyether ether ketone (PEEK) which is a high-performance thermoplastic known for its excellent mechanical and chemical properties, making it suitable for use in experimental setups involving fluid flow and pressure [32]. Using a PEEK core holder offers researchers several advantages, including resistance to chemicals, tolerance for high temperatures, strong mechanical properties, effective electrical insulation, and dimensional stability [63]. These benefits enhance the dependability and precision of streaming potential measurements conducted during core flooding experiments [64]. The pumps (500D Hastelloy Teledyne ISCO pumps, flow rate resolution ~ 0.5% of setpoint, pressure resolution within 0.1% full scale) were used to apply an overburden pressure of 3.45 MPa and a pore back pressure of 1.72 MPa; brine was then injected through the sample at different flow rates (1 ml/min, 2 ml/min, and 3 ml/min) to equilibrate the rock core sample with the brine (note: the core sample was vacuumed before saturating it with brine to avoid air trapping). The back-pressure pump plays a crucial role in streaming core flooding experiments by providing controlled flow rate, representative sampling, continuous collection, and enhanced efficiency during the collection of brine or effluent fluid. The pressure control system (including pumps and pressure gauges) controls the flow rate and pressure of the brine flowing through the core. Two non-polarizing Ag/AgCl electrodes are connected to a high impedance voltmeter to monitor the voltage of the brine. This brine flow through the rock resulted in pressure differential and voltage between the two sides of the core; and flow was continued until stable pressure differential and stable voltage were achieved. This was followed by a system relaxation (i.e. a static state without flow) and the associated static voltage (with zero pressure differential) was recorded. This process was repeated for different pore pressures (up to 6.9 MPa) and overburden pressures (up to 10.34 MPa) at the prescribed temperatures (note that the effective stress, i.e. the difference between overburden and pore back pressures was set to a constant 3.45 MPa [64]). All the pressure and voltage values were recorded and analyzed by a data acquisition system.

2.3. Data analysis

The associated streaming potential coupling coefficient (C_{sp}) and zeta potential (ζ_{sp}) were calculated with the paired stabilization method described in [60]; thus [59]:

$$C_{sp} = \frac{\Delta V}{\Delta P}, \tag{1}$$

where ΔV is the stabilized voltage (in mV) and ΔP is the stabilized pressure differential (in MPa). Note that C_{sp} is therefore the slope of stabilized ΔV plotted versus stabilized ΔP (for varying flow rates, here 1

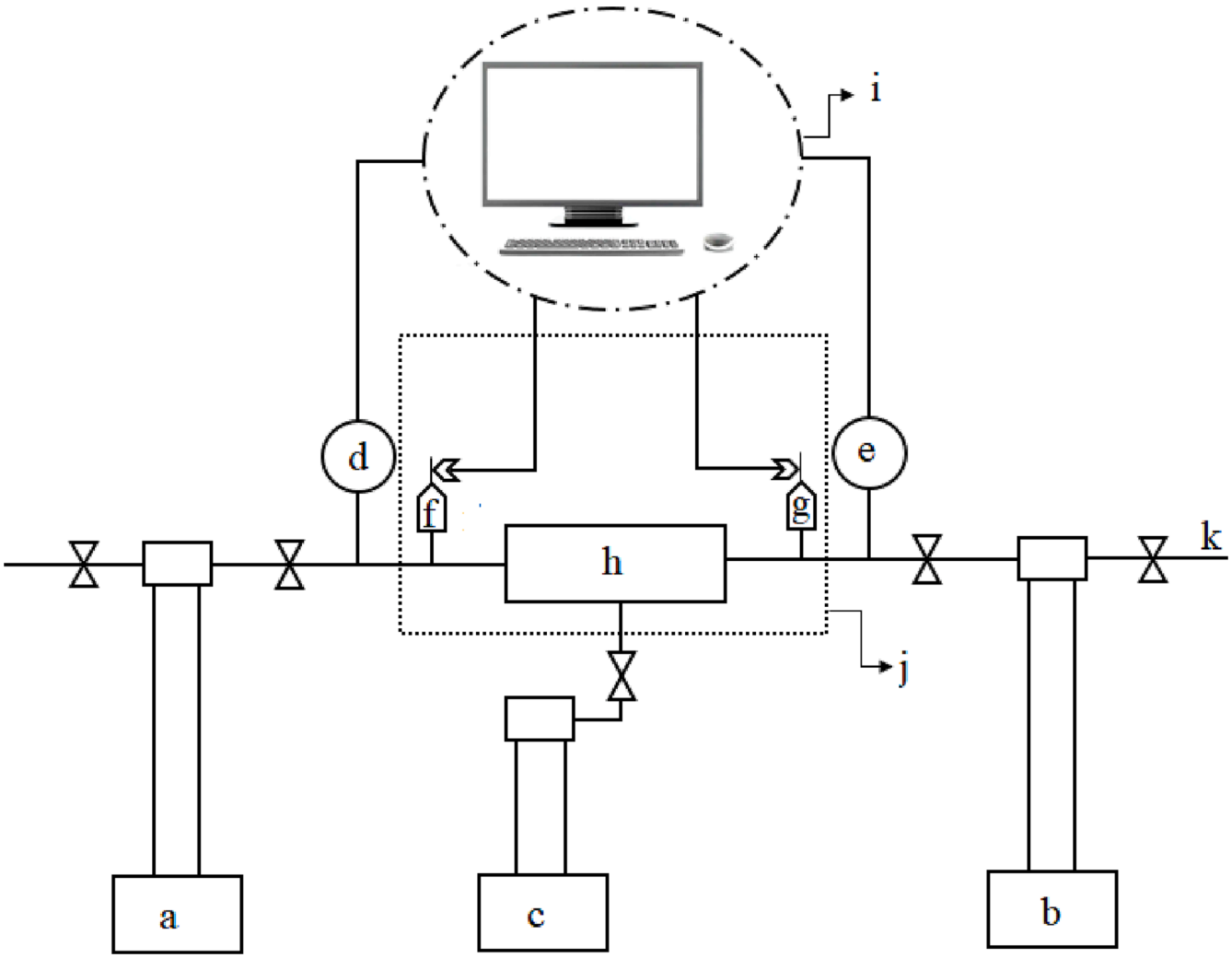

Fig. 1. Experimental apparatus for streaming potential measurements used in this study: (a) ISCO pump (flow rate accuracy of 0.5% of setpoint, pressure accuracy within 0.1% full scale) for injecting brine, (b) ISCO back-pressure pump for collecting brine, (c) ISCO pump for applying overburden pressure, (d) high precision pressure transducer (Keller-Druck, 0.1% accuracy) for monitoring the inlet pressure, (e) high precision pressure transducer for monitoring the outlet pressure, (f) nonpolarizing Ag/AgCl electrode (accuracy 0.15%) at injection side, (g) nonpolarizing Ag/AgCl electrode at collection side, (h) core holder, (i) data acquisition system, (j) oven, (k) effluent collection line.

ml/min, 2 ml/min, and 3 ml/min) at constant pH, brine salinity (S), overburden pressure, pore back pressure (p), and temperature (T) [65]. Fig. 2 shows an example of how C_{sp} was determined at $p = 3.45$ MPa, $T = 323$ K, $S = 1$ wt% NaCl, and brine pH = 7.

The conductivity of a core saturated with water (σ_{rw}) can be calculated using the differential effective medium (DEM) theory [66,67]:

$$\sigma_{rw} = \frac{\sigma_w}{F}\left(\frac{1-\sigma_s/\sigma_w}{1-\sigma_s/\sigma_{rw}}\right)^m, \tag{2}$$

where σ_w is the water conductivity (here obtained from [68]), F is the formation factor, σ_s is the rock surface conductivity, and m is the cementation exponent. Assuming that the effect of surface conductivity is negligible (when compared to the bulk fluid conductivity – i.e. no additional conductivity occurs in the vicinity of the charged interface and the effective conductivity equals the fluid conductivity, resulting in a constant F for all single-phase experiments [44]), which is justified as higher ionic strength (typically for salinities > 0.1 M if the rock contains minerals other than clays [62]), the following equation is obtained [69]:

$$F = \frac{\sigma_w}{\sigma_{rw}}. \tag{3}$$

Thus, ζ_{sp} could be obtained via the classical Helmholtz-Smoluchowski equation [70]:

$$\zeta_{sp} = \frac{\mu_w \sigma_w C_{sp}}{\varepsilon_w}, \tag{4}$$

where μ_w is the dynamic brine viscosity (here obtained from [71]), $\mathcal{E}_w$ is the brine permittivity (here obtained from [71]), and C_{sp} is obtained from Eq. (1), see above. The average standard deviation of C_{sp} and ζ_{sp} were ± 0.3 mV/MPa and ± 2.5 mV based on replicate measurements.

3. Results and discussion

All measured C are given in Table 2 and Fig. 3. In the following, the effect of each thermophysical parameter is discussed in detail.

3.1. Effects of pressure and temperature

Basaltic rock can be found at shallow (near to surface) or deep (i.e. up to 200 km) depth, resulting in a wide range of pore pressures existing in the rock [72]. However, for CGS and geothermal purposes, the ideal production depth lies within 200 to 1000 m underground depth (mostly due to limitations/complications in drilling operations, including slow penetration rate, drill bit and string stuck due to pressure differential

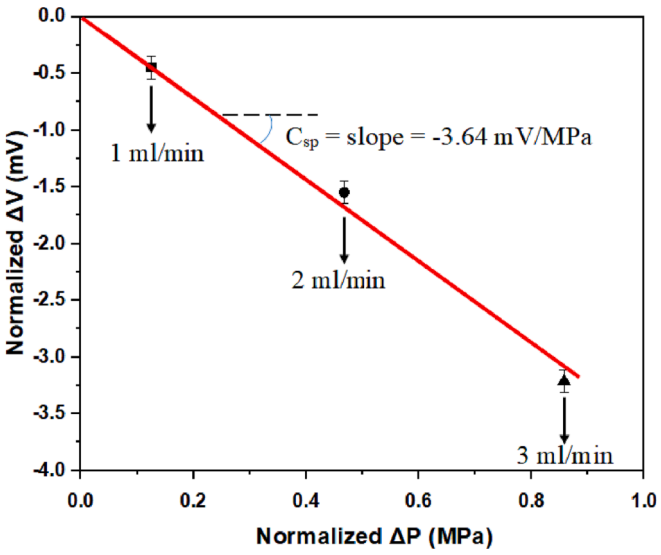

Fig. 2. C_{sp} (curve slope) determined via plotting ΔV versus ΔP (for 1 ml/min, 2 ml/min, and 3 ml/min brine flow rates) at 3.45 MPa, 323 K, 1 wt% NaCl brine salinity at pH = 7.

Table 2
Streaming and zeta potentials measured for basalt.

Brine	p, MPa	T, K	S, wt% NaCl	pH[1]	pH[2]	C, mV/MPa	ζ, mV
Dead	1.72	298	1	7.0	7.1	−9.6	−23.3
Dead	3.45	298	1	7.0	7.3	−9.5	−23.1
Dead	5.17	298	1	7.0	7.4	−9.1	−22.0
Dead	6.9	298	1	7.0	7.3	−9.2	−22.3
Dead	1.72	323	1	7.0	7.0	−3.2	−8.2
Dead	3.45	323	1	7.0	7.1	−3.6	−9.3
Dead	5.17	323	1	7.0	7.3	−3.6	−9.1
Dead	6.9	323	1	7.0	7.2	−3.3	−8.6
Dead	5.17	323	1	4.0	6.4	−1.4	−3.7
Dead	5.17	323	1	8.5	7.4	−4.8	−12.3
Dead	5.17	323	1	10.0	7.9	−6.6	−16.9
Dead	5.17	323	1.8	7.0	7.0	−2.0	−8.2
Dead	5.17	323	2.6	7.0	7.1	−0.7	−4.6
Dead	5.17	323	3.5	7.0	7.2	−0.1	−0.7
Live	5.17	323	1	7.0	5.8	−2.5	−6.3

[1] injected brine at atmospheric condition.
[2] collected brine at atmospheric condition.

between wellbore mud pressure and pore pressure, wellbore collapse, among others [73]). Thus, in this study, we examined a pressure range of 1.72 MPa to 6.9 MPa to mimic realistic underground pressures for gas geo-storage purposes [2].

Dead brine C did not change with pore pressure (at constant temperature, salinity and pH), Table 2 and Fig. 3. Moreover, ζ remained constant when pore pressure increased from 1.72 MPa to 6.9 MPa (at constant temperature), Fig. 4; this behavior was also observed for sandstone (e.g. [19,59]) and carbonates (e.g. [34]); note that for dead brine at constant salinity (here 1 wt% NaCl) and constant temperature (here 298 or 323 K), μ_w, σ_w, and $\mathcal{E}_w$ and also pH remained constant [59,71,74]. However, it was found by [59] that for live brine (where pH decreased with increase in pore pressure due to increased CO_2 dissolution, reaction with water and associated increased acidity, e.g. [75–77]), ζ increased with pore pressure due to protonation of functional surface groups on the rock (e.g. [35,59,74,78,79]). This observation significantly impacts the wettability of CO_2-basalt (which increases with pressure, consistent with the more hydrophobic rock surface characteristics [80,81]). The increase in CO_2-basalt wettability with increase in pressure can also be attributed to the increased intermolecular forces between basalt and CO_2 [82].

Furthermore, C and ζ increased with temperature (decrease in |C| and |ζ|). For example, when temperature increased from 298 K to 323 K at 5.17 MPa, C and ζ changed from −9.1 mV/MPa to −3.6 mV/MPa and from −22 mV to −9.1 mV, respectively. This result is again similar to the responses observed for sandstone (e.g. [35,59,74]) and carbonates (e.g. [32–34]), and is attributed to the decrease in pH when temperature increases at low ionic strength (Note that this is caused by dissociation of water molecules which are more vibrated and ionized at higher temperature, resulting in an increase in hydronium ions and consequently an acidic behavior), [74,83]. Moreover, $\mathcal{E}_w$ and μ_w decreased with temperature, while σ_w increased with temperature (i.e. by increasing temperature from 298 K to 323 K, σ_w increased from 17.83 mS/m to 27.29 mS/mv (see Eq. (9) in [68]), while $\mathcal{E}_w$ decreased from 6.64×10^{-10}F/m to 5.96×10^{-10}F/m (see Eq. (A-3) in [71]) and μ_w decreased from 9.02×10^{-4} Pa.s to 5.58×10^{-4} Pa.s (see Eq. (A-9) in [71]) for dead brine (with a salinity of 1 wt% NaCl at 5.17 MPa). Thus, based on Eq. (4), μ_w and C are the most significant parameters affecting ζ and leading to its increase with temperature. We also conclude that the increase in CO_2 wettability with temperature (for the basalt/CO_2/brine system, e.g. [80,81]) can at least partially be attributed to the decrease in |ζ| with increasing temperature, see Fig. 4.

3.2. Effect of salinity

C and ζ increased with salinity, Fig. 5; for example, when salinity increased from 1 wt% NaCl to 3.5 wt% NaCl at 5.7 MPa and 323 K, C increased from −3.6 mV/MPa to −0.1 mV/MPa, while ζ changed from −9.1 mV to −0.7 mV. However, ζ remained negative over the whole salinity range tested. Such a decrease in |ζ| with increasing salinity was also reported for sandstone (e.g. [29–31,64,65]) and carbonates (e.g. [18,28,33]), albeit anomalies regarding the salinity dependence of ζ have also been reported for sandstone (e.g. [59,84]); those anomalies were attributed to other minerals such as chlorites, montmorillonite, mica, feldspars, and ilmenite contained in the sandstone [51]. Mechanistically this ρ-s response implies that alterations in the electrical resistivity (ρ) of the rock are related to the compression of the electric double layer and the subsequent surface charge (s) shielding (i.e. the negative surface charge of basalt is shielded by the cations of the dissolved salt; note that as the double layer compresses, the ions in the diffuse layer move closer to the surface, leading to increased shielding of the surface charges on the basalt [85,86]), which results in a more electrically neutral surface. Moreover, $\mathcal{E}_w$, decreased with salinity, but μ_w and σ_w increased with salinity. For example, when salinity increased from 1 wt% NaCl to 3.5 wt% NaCl (at $p = 5.17$ MPa and $T = 323$ K), σ_w increased from 27.28 mS/m to 83.08 mS/m, while $\mathcal{E}_w$ slightly decreased from 5.96×10^{-10}F/m to 5.36×10^{-10}F/m and μ_w slightly increased from 5.58×10^{-4} Pa.s to 5.77×10^{-4} Pa.s (for the latter three parameters dead brine with 1 wt% NaCl salinity was considered). Thus, based on Eq. (4), C is the most significant parameter which reduces |ζ| when salinity increases. Consequently, CO_2 wettability increases with salinity for basalt due to the decrease in |ζ| with increasing salinity, see Fig. 5.

Divalent ions found in salts such as Mg^{2+} and Ca^{2+} exhibit stronger electrostatic interactions with the surface of the basaltic rock when compared to monovalent ions such as K^+ and Na^+ [87,88]. These interactions lead to a decrease in the magnitude of the zeta potential [89]. Moreover, certain salts, such as Na_2CO_3, KOH, $(NH_4)_2SO_4$ and KHP have the ability to alter the pH of the brine [90,91]. These pH changes impact the zeta potential of basaltic rocks [29]. In the presence of hydroxyl ions (OH^-), creating alkaline conditions (e.g. by Na_2CO_3 and KOH), the zeta potential becomes more negative [92]. Conversely, the presence of hydrogen ions (H^+), leading to acidic conditions (e.g. by $(NH_4)_2SO_4$ and KHP), leads to less negative zeta potentials [93], see also section 3.3.

3.3. Effect of pH value

In case of CGS, the pH value of the pore fluid in the basalt can vary

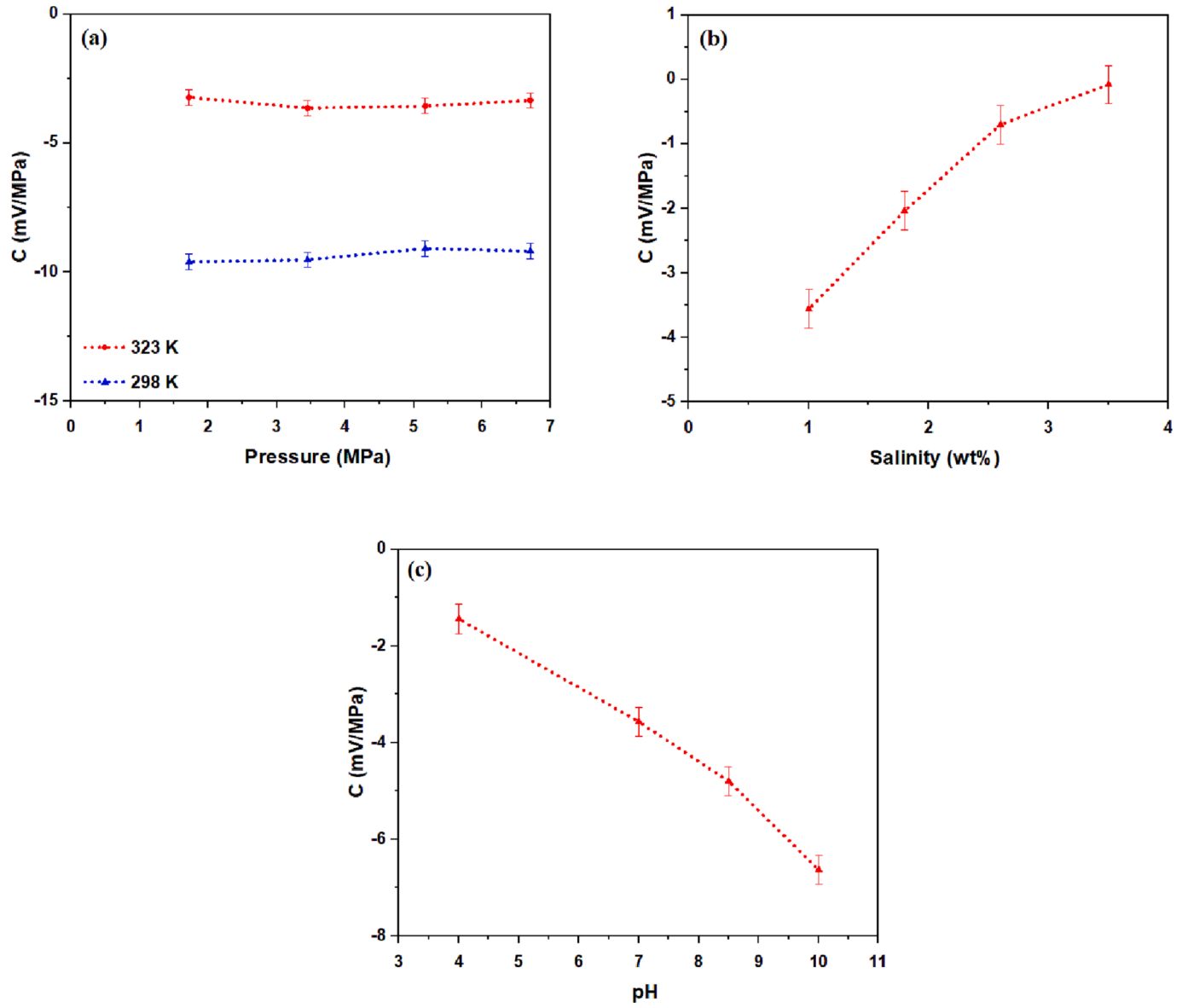

Fig. 3. Streaming potential C of basalt as a function of various thermophysical parameters: (a) effect of pressure and temperature, (b) effect of NaCl concentration (measured at 5.17 MPa and 323 K for dead brine), and (c) effect of pH value of the brine (measured at 1 wt% NaCl concentration, 5.17 MPa, and 323 K for dead brine).

significantly, from relatively low (pH = 3–4 [93–96]) to high (pH = 8–11, due to the basic nature of basalt which contains 45 to 55% silica (i.e. mafic minerals, plagioclase feldspars and feldspathoid minerals, e.g. [97]). Here, C and ζ increased strongly with decreasing pH, as expected (consistent with data reported [29,30,35,51,59] for sandstone and [22,39,40,98,99] for carbonates), and due to protonation of surface function groups (compare reaction schemes 1 and 2, Fig. 6); for instance, C increased from −6.6 mV/MPa to −1.4 mV/MPa and ζ increased from −16.9 mV to −3.7 mV when pH decreased from 10 to 4 (moving pH away from point of zero charge or PZC = 3.5 for basalt [100]). Again, ζ remained negative over the whole pH range tested here, consistent with literature data (reported for other minerals, e.g. [29,59,74]). Overall alkaline components in the basalt (e.g. calcium, magnesium, sodium and potassium which create pH > 7, [92,101]) reduce the surface potential (i.e. render it more negative, by adding OH^- ions onto the rock surface (i.e. via deprotonation reaction, see Scheme 2) while the acidic components (e.g. iron and aluminum which create pH < 7, [93,102]) increase ζ by adding protons (H^+) onto the rock surface (i.e. via a protonation reaction, see Scheme 1).

In addition, in CGS, dissolution trapping is a major storage mechanism, and generally CO_2 mixes with H_2O around the edges of the injected CO_2 plume which (see above) creates acidic live brine [75,103–106]. Thus, we conducted one test for 1 ml/min, 2 ml/min, and 3 ml/min brine flow rates with live brine (1 wt% NaCl brine equilibrated with CO_2 at 5.17 MPa and 323 K) and compared the result with that of dead brine (at the same test pressure and temperature). Now, while C was −3.6 mV/MPa and ζ was −9.1 mV for dead brine (pH = 7.3 for produced brine at atmospheric condition, see Table 2), C = −2.5 mV/MPa and ζ = −6.33 mV were measured for live brine (pH = 5.8 for produced brine at atmospheric condition, see Table 2). This higher ζ for live brine is consistent with our results in terms of the effects of pH on ζ, see above, and it is also consistent with [19,59] where they tested these effects on San Saba sandstone sample at 4.5 to 10 MPa and 298 to 313 K and compared their results with Fontainebleau sample at the same experimental conditions.

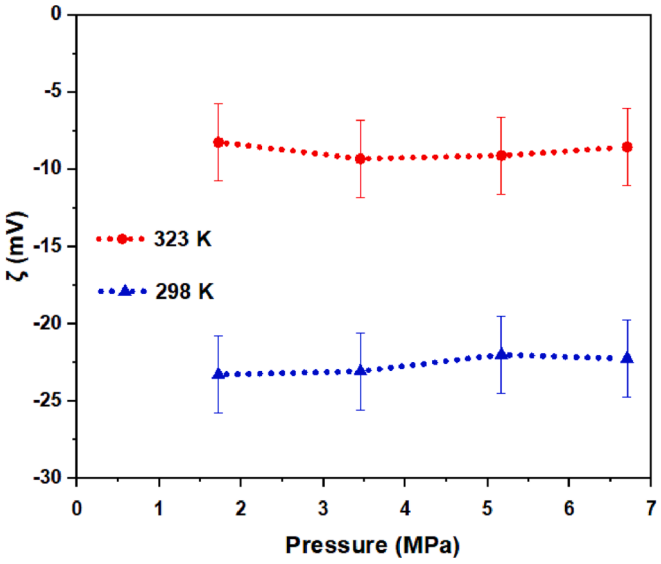

Fig. 4. Zeta potential of the dead brine-basalt system as a function of pore pressure and temperature (measured at 1 wt% NaCl and pH = 7).

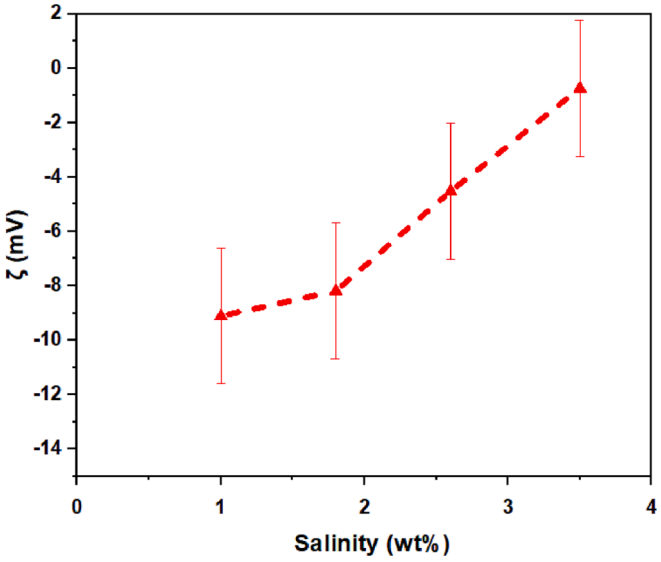

Fig. 5. Basalt zeta potential as a function of NaCl concentration in the dead brine (measured at p = 5.17 MPa, T = 323 K and pH = 7).

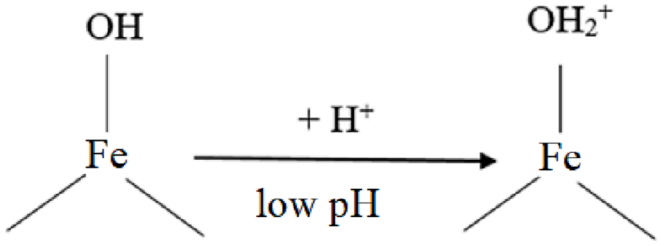

Scheme 1. Protonation of FeOH surface group.

3.4. *Effect of rock mineralogy*

Rock mineralogy significantly affects ζ [64], and it has been suggested that ζ can be estimated as a weighted average of the zeta potentials of all minerals in the rock [30]. Consequently, ζ of the rock is mostly determined by the ζ of the dominant minerals in that rock [59]. For example, in the basalt studied here, the dominant minerals were labradorite and augite (constituting a total of 79.5 wt% of the rock, see Table 1); thus, it is expected that ζ of the basalt is mostly affected by ζ of these two minerals.

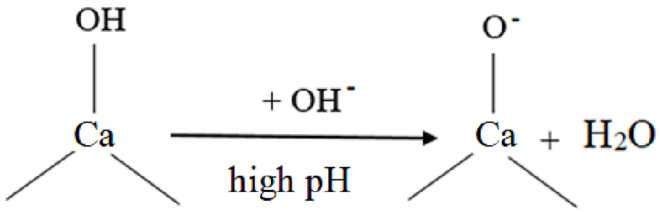

Scheme 2. Deprotonation of CaOH surface group.

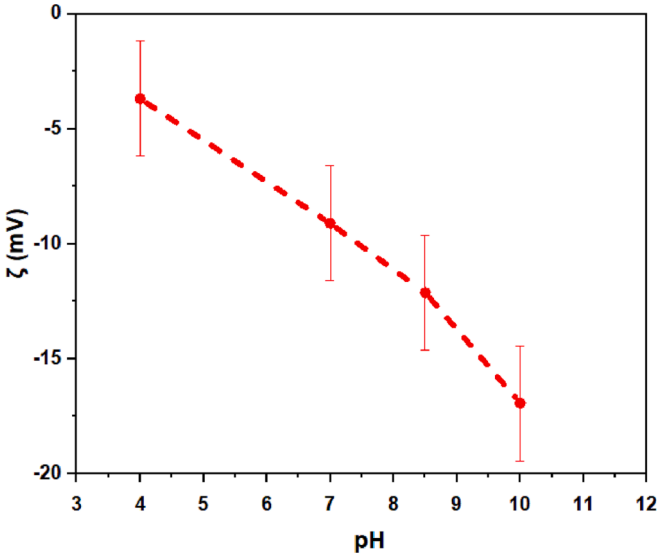

Fig. 6. Zeta potential of basalt as a function of pH value of the brine (measured at 1 wt% NaCl concentration, 5.17 MPa and 323 K).

Augite (a pyroxene mineral which constitutes 37.5 wt% of the basalt) tends to exhibit a negative zeta potential, under typical experimental conditions [49]. This is primarily attributed to the presence of negatively charged surface groups or sites (e.g. silicate groups) on its surface. These silicate groups can undergo ionization in an aqueous environment, resulting in the release of OH^- ions or other negatively charged species [107]. Under neutral to alkaline pH conditions, the dissociation of silicate groups on the augite surface contributes to a net negative charge [108]. Tohry et al. (2021) [47] found that ζ of hematite is more negative than that of augite ($|\zeta_{augite}|<|\zeta_{hematite}|$). Moreover, Forbes and Franks (2013) [109] found that ζ of quartz is more negative than that of hematite ($|\zeta_{hematite}|<|\zeta_{quartz}|$). We, thus, expect that ζ of quartz should be more negative than that of augite ($|\zeta_{augite}|<|\zeta_{quartz}|$).

Similarly, the zeta potentials of labradorite (a plagioclase feldspar which constitutes 42 wt% of the basalt) and nepheline (a feldspathoid mineral which constitutes 8.6 wt% of the basalt) are negative under typical experimental conditions [49,110], indicating their propensity to attract and interact with positively charged species (cations) in the surrounding solution. This can be attributed to the presence of charged surface groups on the mineral surfaces, which are usually derived from the dissociation of OH groups on the surface of the minerals [107].

Despite augite, labradorite and nepheline which tend to exhibit negative ζ, olivine (a magnesium iron silicate which constitutes 11.9 wt % of the basalt) has positive ζ at pH = 5 to 7 [48], resulting in an increase in ζ for basalt.

Overall, ζ of quartz is found to be more negative than that of the

dominant minerals in the basalt, such as labradorite (e.g. as shown in [29] compared to [49]) and augite (as mentioned above). Additionally, ζ of olivine is positive. Therefore, based on these findings, we can conclude that in a macro-scale, ζ_{quartz} is more negative than ζ_{basalt}. It is also important to note that since the SiO_2 content in basalt (i.e. 52 wt%) is less than that of quartz [111], ζ_{quartz} is more negative than ζ_{basalt} [44], which is consistent with literature results (e.g. [109,112,113]) and our result in this study (e.g. see Figs. 4, 5 and 6 for basalt and sandstone). Consequently, more gas wettability of basalt/gas/brine system is expected compared to that of quartz/gas/brine system (e.g. [2,81,114]) due to less $|\zeta|$ in the basalt.

Table 3 lists concentrations of the main cations in the dead and live effluents. In this regard, identification of the dissolved Na is impossible as it is hard to distinguish between Na in NaCl aqueous solution and the dissolved Na. However, it is clearly seen a significant increase in concentration of Ca and carbonate ($CaCO_3$) mineral and a non-significant increase in concentration of Fe and K by the live brine (pH = 5.8) compared to the dead brine (pH = 7.3), implying more dissolution of the minerals by the live brine. This shows the impact of a pH < 7 environment on the mineral dissolution, where divalent cations (e.g. Mg^{2+}, Ca^{2+}, and Fe^{2+}) are released into the solution [115,116] (note that the dissolution rate of basalt is a function of pH and temperature [117]). The release of Ca^{2+} cations as an alkali component of the basalt reduces the pH of the system, implying the less negative zeta potential with the live brine compared to the dead brine. It is notable that high concentration of the divalent cations can enhance the rate of carbon mineralization [118], indicating that the studied basalt can be a good host rock for mineral trapping of CO_2. Furthermore, the permeability and porosity of the basaltic host rock can be increased due to the more mineral dissolution through the live brine [119], resulting in an increase in the streaming potential coupling coefficient, consistent with [42].

4. Conclusions

The electric surface charge of basaltic rocks saturated with geo-fluids (e.g. water, CO_2 and H_2) has many applications in various fields such as CO_2 and H_2 geological storage sites, hydrocarbon reservoirs, and geothermal systems [18–20,23]. Therefore, the zeta potential of a basaltic rock (saturated with aqueous NaCl solutions) was deduced from streaming potential measurement and the effects of pore pressure, temperature, salinity, rock mineralogy and pH were reported for the first time. The key findings of the study are as follows:

- ζ was negative at all thermophysical conditions examined in this study; the ζ of dead brine remained constant versus pore pressure (as the pH value did not change). However, ζ strongly increased when CO_2 was added (and pH decreased significantly, live brine); thus the magnitude of ζ decreased with pore pressure when CO_2 was present, implying an increase in CO_2 wettability with pore pressure, and consistent with independent contact angle measurements (e.g. [80,81]).
- ζ increased (attained less negative values) with increasing temperature (implying an increase in CO_2 wettability with temperature, consistent with literature [2,80,81,120]) and salinity, but decreased (became more negative) with increasing pH.
- Pore pressure, temperature and salt type have an indirect impact on the ζ via impact on pH, while the pH value strongly affects ζ [19,29,38].
- The ζ_{basalt} measured in this study is less negative than $\zeta_{sandstone}$ reported in the literature (i.e. ζ_{basalt} = -9.53 mV/MPa and $\zeta_{sandstone}$ = -15.7 mV/MPa at p = 3.45 MPa, T = 298 K, pH = 7 and S = 1 wt% NaCl were obtained, e.g. [19]).

The fundamental results reported in this study are relevant for many applications, including gas geo-storage (CO_2 and H_2), subsurface flow pattern interpretation and geothermal projects.

Table 3
Concentrations of the main cations in the dead and live brines.

Element	Unit	Live brine	Dead brine
Ca	mg/L	1.1	< 0.5
Mg	mg/L	< 0.5	< 0.5
K	mg/L	2.0	1.9
Na	mg/L	3800	3800
Fe	μg/L	19	< 10
Hardness as $CaCO_3$*	mg/L	4.9	< 3.0

* The released Ca^{2+} cations into the solution can react with dissolved CO_2 to form carbonate ($CaCO_3$) mineral [104].

CRediT authorship contribution statement

Mirhasan Hosseini: Conceptualization, Methodology, Investigation, Writing – original draft. **Faisal Ur Rahman Awan:** Visualization, Methodology, Writing – review & editing. **Nilesh Kumar Jha:** Formal analysis, Methodology, Writing – review & editing. **Alireza Keshavarz:** Resources, Supervision, Writing – review & editing. **Stefan Iglauer:** Validation, Writing – review & editing, Supervision.

Declaration of Competing Interest

The authors declare that they have no known competing financial interests or personal relationships that could have appeared to influence the work reported in this paper.

Data availability

No data was used for the research described in the article.

Acknowledgments

This research was supported by the Australian Government through the Australian Research Council's Discovery Projects funding scheme (project DP220102907).

References

[1] Gislason SR, Wolff-Boenisch D, Stefansson A, Oelkers EH, Gunnlaugsson E, Sigurdardottir H, et al. Mineral sequestration of carbon dioxide in basalt: a pre-injection overview of the CarbFix project. Int J Greenhouse Gas Control 2010;4(3):537–45.
[2] Hosseini M, Ali M, Fahimpour J, Keshavarz A, Iglauer S. Basalt-H2-brine wettability at geo-storage conditions: Implication for hydrogen storage in basaltic formations. J Storage Mater 2022;52:104745.
[3] le Roex A. Mid-ocean ridge basalt (MORB). Geochem Encyclopedia Earth Sci 1998.
[4] Hosseini M, Ali M, Fahimpour J, Keshavarz A, Iglauer S. Assessment of rock-hydrogen and rock-water interfacial tension in shale, evaporite and basaltic rocks. J Nat Gas Sci Eng 2022;106:104743.
[5] Ren K, Zhao J, Liu Q, Zhao J. Hydrocarbons in igneous rock of Brazil: a review. Pet Res 2020;5(3):265–75.
[6] Schutter SR. Occurrences of hydrocarbons in and around igneous rocks. Geol Soc Lond Spec Publ 2003;214(1):35–68.
[7] Eidesgaard Ó, Schovsbo N, Boldreel L, Ólavsdóttir J. Shallow geothermal energy system in fractured basalt: a case study from Kollafjørður, Faroe Islands. NE-Atlantic Ocean Geothermics 2019;82:296–314.
[8] Khadri S, Moharir K. Characterization of aquifer parameter in basaltic hard rock region through pumping test methods: a case study of Man River basin in Akola and Buldhana Districts Maharashtra India. Modeling Earth Systems Environ 2016;2(1):1–18.
[9] Möller P, Rosenthal E, Inbar N, Magri F. Hydrochemical considerations for identifying water from basaltic aquifers: the Israeli experience. J Hydrol: Reg Stud 2016;5:33–47.
[10] Ystroem LH, Nitschke F, Held S, Kohl T. A multicomponent geothermometer for high-temperature basalt settings. Geothermal Energy 2020;8(1):1–21.
[11] Orywall P, Drüppel K, Kuhn D, Kohl T, Zimmermann M, Eiche E. Flow-through experiments on the interaction of sandstone with Ba-rich fluids at geothermal conditions. Geothermal Energy 2017;5(1):1–24.
[12] Samaniego V, Chilingarian G, Mazzullo S, Rieke H. Chapter 10 Fluid Flow Through Carbonate Rock Systems. Carbonate Reservoir Characterization: A Geologic-Engineering Analysis. Part I. Elsevier, NewYork; 1992.

[13] Zhou X, Karimi-Fard M, Durlofsky LJ, Aydin A. Fluid flow through porous sandstone with overprinting and intersecting geological structures of various types. Geol Soc Lond Spec Publ 2014;374(1):187–209.
[14] Zhou Xu, Zhang Q, Xing H, Lv J, Su H, Huang Z. Numerical study of reactive flow in fractured carbonate rock. Front Earth Sci 2021;9.
[15] Passarella M. Basalt-fluid interactions at subcritical and supercritical conditions: An experimental study. Open Access Te Herenga Waka-Victoria University of Wellington; 2021.
[16] Zeta HRJ. potential in colloid science: principles and applications. Academic press; 2013.
[17] Sprunt ES, Mercer TB, Djabbarah NF. Streaming potential from multiphase flow. Geophysics 1994;59(5):707–11.
[18] Collini H, Li S, Jackson MD, Agenet N, Rashid B, Couves J. Zeta potential in intact carbonates at reservoir conditions and its impact on oil recovery during controlled salinity waterflooding. Fuel 2020;266:116927.
[19] Hidayat M, Sarmadivaleh M, Derksen J, Vega-Maza D, Iglauer S, Vinogradov J. Zeta potential of CO2-rich aqueous solutions in contact with intact sandstone sample at temperatures of 23° C and 40° C and pressures up to 10.0 MPa. J Colloid Interface Sci 2022;607:1226–38.
[20] Jackson MD, Al-Mahrouqi D, Vinogradov J. Zeta potential in oil-water-carbonate systems and its impact on oil recovery during controlled salinity water-flooding. Sci Rep 2016;6(1):1–13.
[21] Leinov E, Jackson M. Experimental measurements of the SP response to concentration and temperature gradients in sandstones with application to subsurface geophysical monitoring. J Geophys Res Solid Earth 2014;119(9):6855–76.
[22] Mahani H, Keya AL, Berg S, Nasralla R. Electrokinetics of carbonate/brine interface in low-salinity waterflooding: Effect of brine salinity, composition, rock type, and pH on?-potential and a surface-complexation model. SPE J 2017;22(01):53–68.
[23] Revil A, Pezard P. Streaming electrical potential anomaly along faults in geothermal areas. Geophys Res Lett 1998;25(16):3197–200.
[24] Awan FUR, Keshavarz A, Akhondzadeh H, Al-Anssari S, Al-Yaseri A, Nosrati A, et al. Stable dispersion of coal fines during hydraulic fracturing flowback in coal seam gas reservoirs—an experimental study. Energy Fuel 2020;34(5):5566–77.
[25] Arif M, Abu-Khamsin SA, Iglauer S. Wettability of rock/CO2/brine and rock/oil/CO2-enriched-brine systems: Critical parametric analysis and future outlook. Adv Colloid Interface Sci 2019;268:91–113.
[26] Luong DT, Rudolf S. Zeta potential measurement using streaming potential in porous media. VNU J Scie: Math-Phys 2015;31(4).
[27] Singh N, Gopani PH, Sarma HK, Mattey P, Negi DS, Srivastava VR, et al. Charging behaviour at the carbonate rock-water interface in low-salinity waterflooding: Estimation of zeta potential in high-salinity brines. Can J Chem Eng 2022;100(6):1226–34.
[28] Cherubini A, Garcia B, Cerepi A, Revil A. Streaming potential coupling coefficient and transport properties of unsaturated carbonate rocks. Vadose Zone J 2018;17(1):1–12.
[29] Walker E, Glover P. Measurements of the relationship between microstructure, pH, and the streaming and zeta potentials of sandstones. Transp Porous Media 2018;121(1):183–206.
[30] Alarouj M, Collini H, Jackson MD. Positive zeta potential in sandstones saturated with natural saline brine. Geophys Res Lett 2021;48(20).
[31] Nasralla RA, Nasr-El-Din HA. Impact of cation type and concentration in injected brine on oil recovery in sandstone reservoirs. J Pet Sci Eng 2014;122:384–95.
[32] Al Mahrouqi D, Vinogradov J, Jackson MD. Temperature dependence of the zeta potential in intact natural carbonates. Geophys Res Lett 2016;43(22).
[33] Al Mahrouqi D, Vinogradov J, Jackson MD. Zeta potential of artificial and natural calcite in aqueous solution. Adv Colloid Interface Sci 2017;240:60–76.
[34] Rodríguez K, Araujo M. Temperature and pressure effects on zeta potential values of reservoir minerals. J Colloid Interface Sci 2006;300(2):788–94.
[35] Vinogradov J, Jackson MD. Zeta potential in intact natural sandstones at elevated temperatures. Geophys Res Lett 2015;42(15):6287–94.
[36] Revil A, Cerepi A. Streaming potentials in two-phase flow conditions. Geophys Res Lett 2004;31(11):n/a–.
[37] Alroudhan A, Vinogradov J, Jackson M. Zeta potential of intact natural limestone: impact of potential-determining ions Ca, Mg and SO4. Colloids Surf A Physicochem Eng Asp 2016;493:83–98.
[38] Thanh LD, Sprik R. Zeta potential in porous rocks in contact with monovalent and divalent electrolyte aqueous solutions. Geophysics 2016;81(4):D303–14.
[39] Vdović N, Bišćan J. Electrokinetics of natural and synthetic calcite suspensions. Colloids Surf A Physicochem Eng Asp 1998;137(1–3):7–14.
[40] Vdović N. Electrokinetic behaviour of calcite—the relationship with other calcite properties. Chem Geol 2001;177(3–4):241–8.
[41] Chen L, Zhang G, Wang L, Wu W, Ge J. Zeta potential of limestone in a large range of salinity. Colloids Surf A Physicochem Eng Asp 2014;450:1–8.
[42] Jouniaux L, Bernard ML, Zamora M, Pozzi JP. Streaming potential in volcanic rocks from Mount Pelée. J Geophys Res Solid Earth 2000;105(B4):8391–401.
[43] Ishido T, Mizutani H. Experimental and theoretical basis of electrokinetic phenomena in rock-water systems and its applications to geophysics. J Geophys Res Solid Earth 1981;86(B3):1763–75.
[44] Hase H, Ishido T, Takakura S, Hashimoto T, Sato K, Tanaka Y. ζ potential measurement of volcanic rocks from Aso caldera. Geophys Res Lett 2003;30(23):n/a–.
[45] Reedijk J, Poeppelmeier K. Comprehensive inorganic chemistry II: from elements to applications. In: V1 Main-Group Elem., Incl. Noble Gases V2 Transition Elem., Lanthanides and Actinides V3 Bioinorganic Fundam. and Appl.: Metals in Nat. Living Syst. and Metals in Toxicology and Med. V4 Solid-State Mater., Incl. Ceramics and Minerals V5 Porous Mater. and Nanomaterials V6 Homogeneous Catal. Appl. V7 Surf. Inorganic Chem. and Heterog. Catal. V8 Coord. and Organometallic Chem. V9 Theory and Methods. Elsevier Ltd.; 2013. p. 1–7196.
[46] Aizawa K, Uyeshima M, Nogami K. Zeta potential estimation of volcanic rocks on 11 island arc-type volcanoes in Japan: Implication for the generation of local self-potential anomalies. J Geophys Res: Solid Earth 2008:113(B2).
[47] Tohry A, Dehghan R, Zarei M, Chelgani SC. Mechanism of humic acid adsorption as a flotation separation depressant on the complex silicates and hematite. Miner Eng 2021;162:106736.
[48] Ucbas Y, Bozkurt V, Bilir K, Ipek H. Concentration of chromite by means of magnetic carrier using sodium oleate and other reagents. Physicochem Problems Mineral Processing 2014:50.
[49] Dunning J, Herren B, Tipps R, Snyder R. Fractionation of mineral species by electrophoresis. J Geophys Res Solid Earth 1982;87(B13):10781–8.
[50] Vidyadhar A, Rao KH. Adsorption mechanism of mixed cationic/anionic collectors in feldspar-quartz flotation system. J Colloid Interface Sci 2007;306(2):195–204.
[51] Shehata AM, Nasr-El-Din HA. Zeta potential measurements: Impact of salinity on sandstone minerals. OnePetro: SPE International Symposium on Oilfield Chemistry; 2015.
[52] Bjørlykke K, Gran K. Salinity variations in North Sea formation waters: Implications for large-scale fluid movements. Mar Pet Geol 1994;11(1):5–9.
[53] Hosseini M. Estimation of mean pore-size using formation evaluation and Stoneley slowness. J Nat Gas Sci Eng 2016;33:898–907.
[54] Hosseini M. Formation evaluation of a clastic gas reservoir: presentation of a solution to a fundamentally difficult problem. J Geophys Eng 2018;15(6):2418–32.
[55] Hosseini M, Javaherian A, Movahed B. Determination of permeability index using Stoneley slowness analysis, NMR models, and formation evaluations: a case study from a gas reservoir, south of Iran. J Appl Geophys 2014;109:80–7.
[56] Hosseini M, Ali M, Fahimpour J, Keshavarz A, Iglauer S. Calcite-fluid interfacial tension: h2 and co2 geological storage in carbonates. Energy Fuel 2023;37(8):5986–94.
[57] Hosseini M, Fahimpour J, Ali M, Keshavarz A, Iglauer S. Hydrogen wettability of carbonate formations: Implications for hydrogen geo-storage. J Colloid Interface Sci 2022;614:256–66.
[58] Hosseini M, Fahimpour J, Ali M, Keshavarz A, Iglauer S. Capillary sealing efficiency analysis of caprocks: implication for hydrogen geological storage. Energy Fuel 2022;36(7):4065–75.
[59] Hidayat M, Sarmadivaleh M, Derksen J, Vega-Maza D, Iglauer S, Vinogradov J. Zeta potential of a natural clayey sandstone saturated with carbonated NaCl solutions at supercritical CO2 conditions. Geophys Res Lett 2022;49(15).
[60] Vinogradov J, Jackson MD. Multiphase streaming potential in sandstones saturated with gas/brine and oil/brine during drainage and imbibition. Geophys Res Lett 2011;38(1):n/a–.
[61] Molloy C, Shane P, Augustinus P. Eruption recurrence rates in a basaltic volcanic field based on tephra layers in maar sediments: implications for hazards in the Auckland volcanic field. Geol Soc Am Bull 2009;121(11–12):1666–77.
[62] Weller A, Slater L, Nordsiek S. On the relationship between induced polarization and surface conductivity: Implications for petrophysical interpretation of electrical measurements. Geophysics 2013;78(5):D315–25.
[63] Shakerian M, Balcom B. An MR/MRI compatible core holder with the RF probe immersed in the confining fluid. J Magn Reson 2018;286:36–41.
[64] Awan FUR, Al-Yaseri A, Akhondzadeh H, Iglauer S, Keshavarz A. Influence of mineralogy and surfactant concentration on zeta potential in intact sandstone at high pressure. J Colloid Interface Sci 2022;607:401–11.
[65] Vinogradov J, Jaafar M, Jackson M. Measurement of streaming potential coupling coefficient in sandstones saturated with natural and artificial brines at high salinity. J Geophys Res: Solid Earth 2010:115(B12).
[66] Sen P, Scala C, Cohen M. A self-similar model for sedimentary rocks with application to the dielectric constant of fused glass beads. Geophysics 1981;46(5):781–95.
[67] Sen PN. Grain shape effects on dielectric and electrical properties of rocks. Geophysics 1984;49(5):586–7.
[68] Sen PN, Goode PA. Influence of temperature on electrical conductivity on shaly sands. Geophysics 1992;57(1):89–96.
[69] Li S, Leroy P, Heberling F, Devau N, Jougnot D, Chiaberge C. Influence of surface conductivity on the apparent zeta potential of calcite. J Colloid Interface Sci 2016;468:262–75.
[70] Jouniaux L, Pozzi JP. Streaming potential and permeability of saturated sandstones under triaxial stress: Consequences for electrotelluric anomalies prior to earthquakes. J Geophys Res Solid Earth 1995;100(B6):10197–209.
[71] Saunders J, Jackson M, Gulamali M, Vinogradov J, Pain C. Streaming potentials at hydrocarbon reservoir conditions. Geophysics 2012;77(1):E77–90.
[72] Cas RA, Simmons JM. Why deep-water eruptions are so different from subaerial eruptions. Front Earth Sci 2018;6:198.
[73] Millett JM, Wilkins AD, Campbell E, Hole MJ, Taylor RA, Healy D, et al. The geology of offshore drilling through basalt sequences: understanding operational complications to improve efficiency. Mar Pet Geol 2016;77:1177–92.
[74] Vinogradov J, Jackson MD, Chamerois M. Zeta potential in sandpacks: Effect of temperature, electrolyte pH, ionic strength and divalent cations. Colloids Surfaces A: Physicochem Eng Aspects 2018;553:259–71.
[75] Iglauer S. Dissolution trapping of carbon dioxide in reservoir formation brine-a carbon storage mechanism. UK: INTECH Open Access Publisher London; 2011.

[76] Peng C, Crawshaw JP, Maitland GC, Trusler JM, Vega-Maza D. The pH of CO2-saturated water at temperatures between 308 K and 423 K at pressures up to 15 MPa. J Supercrit Fluids 2013;82:129–37.
[77] Adamczyk K, Prémont-Schwarz M, Pines D, Pines E, Nibbering ET. Real-time observation of carbonic acid formation in aqueous solution. Science 2009;326 (5960):1690–4.
[78] Karunarathne CI, Al-Yaseri AZ, Keshavarz A, Iglauer S. Effect of inorganic acid concentration on sandstone surface chemistry examined via nuclear magnetic resonance. J Phys Chem C 2022;126(26):10863–71.
[79] Stumm W, Morgan JJ. Aquatic chemistry: chemical equilibria and rates in natural waters. John Wiley & Sons; 2012.
[80] Al-Yaseri A, Ali M, Ali M, Taheri R, Wolff-Boenisch D. Western Australia basalt-CO2-brine wettability at geo-storage conditions. J Colloid Interface Sci 2021;603: 165–71.
[81] Iglauer S, Al-Yaseri AZ, Wolff-Boenisch D. Basalt-CO2-brine wettability at storage conditions in basaltic formations. Int J Greenhouse Gas Control 2020;102: 103148.
[82] Iglauer S, Mathew MS, Bresme F. Molecular dynamics computations of brine–CO2 interfacial tensions and brine–CO2–quartz contact angles and their effects on structural and residual trapping mechanisms in carbon geo-sequestration. J Colloid Interface Sci 2012;386(1):405–14.
[83] Ross E, Behringer D. Changes in temperature, pH, and salinity affect the sheltering responses of Caribbean spiny lobsters to chemosensory cues. Sci Rep 2019;9(1):1–11.
[84] Li S, Collini H, Jackson MD. Anomalous zeta potential trends in natural sandstones. Geophys Res Lett 2018;45(20).
[85] Al-Yaseri AZ, Lebedev M, Barifcani A, Iglauer S. Receding and advancing (CO2+ brine+ quartz) contact angles as a function of pressure, temperature, surface roughness, salt type and salinity. J Chem Thermodyn 2016;93:416–23.
[86] Arif M, Lebedev M, Barifcani A, Iglauer S. CO2 storage in carbonates: Wettability of calcite. Int J Greenhouse Gas Control 2017;62:113–21.
[87] Gopani PH, Singh N, Sarma HK, Mattey P, Srivastava VR. Role of monovalent and divalent ions in low-salinity water flood in carbonate reservoirs: an integrated analysis through zeta potentiometric and simulation studies. Energies 2021;14 (3):729.
[88] Salgin S, Salgin U, Bahadir S. Zeta potentials and isoelectric points of biomolecules: the effects of ion types and ionic strengths. Int J Electrochem Sci 2012;7(12):12404–14.
[89] Yukselen-Aksoy Y, Kaya A. A study of factors affecting on the zeta potential of kaolinite and quartz powder. Environ Earth Sci 2011;62(4):697–705.
[90] Xu Z, Zhu W, Gong M, Zhang H. Direct gasification of dewatered sewage sludge in supercritical water. Part 1: effects of alkali salts. Int J Hydrogen Energy 2013;38 (10):3963–72.
[91] Alhakimi G, Studnicki LH, Al-Ghazali M. Photocatalytic destruction of potassium hydrogen phthalate using TiO2 and sunlight: application for the treatment of industrial wastewater. J Photochem Photobiol A Chem 2003;154(2–3):219–28.
[92] Kovalchuk O, Zozulynets V, Semerikov S, Chukharev S, Sakhno S, Striuk A, et al. Study of influence of alkaline component type on pH value and properties of alkali activated concretes containing basalt rock. E3S Web Conf 2021;280:07001.
[93] Gislason SR, Broecker WS, Gunnlaugsson E, Snæbjörnsdóttir S, Mesfin KG, Alfredsson HA, et al. Rapid solubility and mineral storage of CO2 in basalt. Energy Procedia 2014;63:4561–74.
[94] Galeczka I, Wolff-Boenisch D, Gislason S. Experimental studies of basalt-H2O-CO2 interaction with a high pressure column flow reactor: the mobility of metals. Energy Procedia 2013;37:5823–33.
[95] Rogers KL, Neuhoff PS, Pedersen AK, Bird DK. CO2 metasomatism in a basalt-hosted petroleum reservoir, Nuussuaq. West Greenland Lithos 2006;92(1–2): 55–82.
[96] Kaszuba JP, Janecky DR. Geochemical impacts of sequestering carbon dioxide in brine formations. Carbon sequestration and its role in the global carbon cycle 2009;183:239–48.
[97] Gudbrandsson S, Wolff-Boenisch D, Gislason SR, Oelkers EH. An experimental study of crystalline basalt dissolution from 2⩽ pH⩽ 11 and temperatures from 5 to 75 C. Geochim Cosmochim Acta 2011;75(19):5496–509.
[98] Farooq U, Tweheyo MT, Sjöblom J, Øye G. Surface characterization of model, outcrop, and reservoir samples in low salinity aqueous solutions. J Dispers Sci Technol 2011;32(4):519–31.
[99] Saw RK, Mandal A. A mechanistic investigation of low salinity water flooding coupled with ion tuning for enhanced oil recovery. RSC Adv 2020;10(69): 42570–83.
[100] Anda M, Shamshuddin J, Fauziah C. Improving chemical properties of a highly weathered soil using finely ground basalt rocks. Catena 2015;124:147–61.
[101] Bell DR, Rossman GR, Maldener J, Endisch D, Rauch F. Hydroxide in olivine: A quantitative determination of the absolute amount and calibration of the IR spectrum. Journal of Geophysical Research: Solid. Earth 2003;108(B2).
[102] Snæbjörnsdóttir SÓ, Wiese F, Fridriksson T, Ármansson H, Einarsson GM, Gislason SR. CO2 storage potential of basaltic rocks in Iceland and the oceanic ridges. Energy Procedia 2014;63:4585–600.
[103] Riaz A, Hesse M, Tchelepi H, Orr F. Onset of convection in a gravitationally unstable diffusive boundary layer in porous media. J Fluid Mech 2006;548: 87–111.
[104] Raza A, Glatz G, Gholami R, Mahmoud M, Alafnan S. Carbon mineralization and geological storage of CO2 in basalt: Mechanisms and technical challenges. Earth Sci Rev 2022;229:104036.
[105] El-Maghraby R, Pentland C, Iglauer S, Blunt M. A fast method to equilibrate carbon dioxide with brine at high pressure and elevated temperature including solubility measurements. J Supercrit Fluids 2012;62:55–9.
[106] Al-Khdheeawi EA, Vialle S, Barifcani A, Sarmadivaleh M, Iglauer S. Impact of reservoir wettability and heterogeneity on CO2-plume migration and trapping capacity. Int J Greenhouse Gas Control 2017;58:142–58.
[107] Hair ML. Hydroxyl groups on silica surface. J Non Cryst Solids 1975;19:299–309.
[108] Zhuravlev LT. Concentration of hydroxyl groups on the surface of amorphous silicas. Concentration of hydroxyl groups on the surface of amorphous silicas 1987;3(3):316–8.
[109] Forbes E, Franks G. Selective separation of hematite from quartz by flotation using a temperature responsive polymer. Iron Ore 2013:12–4.
[110] Rudolph M, Peuker UA. Mapping hydrophobicity combining AFM and Raman spectroscopy. Miner Eng 2014;66:181–90.
[111] Le Bas M, Streckeisen AL. The IUGS systematics of igneous rocks. J Geol Soc London 1991;148(5):825–33.
[112] Fan G, Wang L, Cao Y, Li C. Collecting agent–mineral interactions in the reverse flotation of iron ore: a brief review. Minerals 2020;10(8):681.
[113] Zhou F, Liu Qi, Liu Xu, Li W, Feng J, Chi R-a. Surface Electrical Behaviors of Apatite, Dolomite, Quartz, and Phosphate Ore. Front Mater 2020;7.
[114] Iglauer S. CO2–water–rock wettability: variability, influencing factors, and implications for CO2 geostorage. Acc Chem Res 2017;50(5):1134–42.
[115] Park A-H-A, Fan L-S. CO2 mineral sequestration: physically activated dissolution of serpentine and pH swing process. Chem Eng Sci 2004;59(22–23):5241–7.
[116] Goldberg DS, Takahashi T, Slagle AL. Carbon dioxide sequestration in deep-sea basalt. Proc Natl Acad Sci 2008;105(29):9920–5.
[117] Gislason SR, Oelkers EH. Mechanism, rates, and consequences of basaltic glass dissolution: II. An experimental study of the dissolution rates of basaltic glass as a function of pH and temperature. Geochim Cosmochim Acta 2003;67(20): 3817–32.
[118] Flaathen TK. Water-rock interaction during CO2 sequestration in basalt. Université Paul Sabatier-Toulouse III; 2009.
[119] Kanakiya S, Adam L, Esteban L, Rowe MC, Shane P. Dissolution and secondary mineral precipitation in basalts due to reactions with carbonic acid. J Geophys Res Solid Earth 2017;122(6):4312–27.
[120] Al-Yaseri A, Jha NK. On hydrogen wettability of basaltic rock. J Pet Sci Eng 2021; 200:108387.